IJHSR
ijhighschoolresearch.org
RESEARCH ARTICLE

Thermoelectric Performance of n-Type Argyrodite Ag_8GeTe_6 with Ultralow Lattice Thermal Conductivity and High Mobility Near Room Temperature

Juyoung Chang[1], Runyu Che[2], Beomjun Kim[3], Chaemin Lee[4], Abhijit Debnath[5], Woo Rin Lee*

1. Seoul Foreign School, Seoul, South Korea 03723
2. Gyeonggi Suwon International School, Gyeonggi-Do, South Korea 16706
3. Seoul International School, Gyeonggi-do, South Korea 13113
4. Phillips Exeter Academy, Exeter, NH 03833-2460 USA
5. IEM, Newtown, University of Engineering and Management, Kolkata, India, 700160.
*gosyber1@gmail.com

ABSTRACT: Polycrystalline Ag_8GeTe_6 was synthesized by solid-state melting and spark plasma sintering, and its thermoelectric properties were investigated from 2 to 380 K. X-ray diffraction confirmed a cubic argyrodite structure with high phase purity, while diffuse reflectance spectra indicated a band gap of ~0.45 eV. Transport measurements revealed a semiconducting-to-metallic transition near 244 K. Hall data showed n-type conduction with carrier concentrations ~1017 cm-3 and exceptionally high room-temperature mobility (~3090 cm2 V-1 s-1). The Seebeck coefficient remained negative, reaching −140 μV/K at 380 K, with a power factor of 74 μWm-1K-2. The thermal conductivity was ultralow (0.13–0.33 $W \cdot m^{-1} \cdot K^{-1}$), dominated by a nearly temperature-independent lattice term arising from disordered Ag cations, consistent with phonon liquid–electron crystal behavior. Heat-capacity analysis confirmed low-energy Einstein modes consistent with localized vibrations. Compared with previous reports, the n-type Ag_8GeTe_6 synthesized in this work exhibits enhanced thermoelectric performance, achieving a maximum ZT of 0.10 at 380 K—approximately twice the previously reported value—due to the synergistic combination of ultralow lattice thermal conductivity, exceptionally high carrier mobility, and reduced electrical resistivity.

KEYWORDS: Materials Science, Thermoelectric Materials, Argyrodite Ag_8GeTe_6, Ultralow Lattice Thermal Conductivity, High Carrier Mobility.

Introduction

The study of thermoelectric (TE) materials has advanced quickly due to the global call for sustainable and environmentally friendly energy sources. TE materials can directly convert thermal gradients into electricity and vice versa, without moving parts or harmful emissions.[1] The efficacy of TE materials is commonly expressed by the dimensionless figure of merit, $ZT = (S^2/\rho\kappa)T$, where S is the Seebeck coefficient, ρ is the electrical resistivity, κ is the total thermal conductivity (which includes both electronic, κ_e, and lattice, κ_l, contributions), and T is the absolute temperature.[2] These parameters are strongly attached to the carrier concentration (n). A high S, low ρ, and low κ are required to achieve a high ZT.[3,4] Therefore, strategies that decouple these parameters are essential for further improvement.

Over the past two decades, several new classes of promising TE materials have been developed, such as skutterudites,[5,6] half-Heuslers,[7,8] and clathrates.[9,10] Approaches to increase the power factor (S^2/ρ) include band structure engineering (band convergence[11,12] and band nesting[13,14]) and the introduction of resonant states.[15,16] Methods to reduce κ involve introducing point defects,[17] and nano-inclusions[18] atomic rattlers,[19] complex crystal structures,[20] and soft phonon modes.[21]

Recently, superionic conductors have emerged as attractive TE materials for medium- to high-temperature applications.[22] Among them, Ag- and Cu-based chalcogenides such as Cu_2Se,[23] Cu_2S,[24] Ag_2Se,[25,26] and CuAgSe[27] have been widely investigated. Their low lattice thermal conductivity (κ_l) is the main factor contributing to high ZT, since κ_l is largely independent of other transport parameters. Superionic conductors typically have two distinct structural sublattices: a rigid anion framework and a disordered cation sublattice.[28,29] This exclusive structure allows partial decoupling of charge and phonon transport. The rigid anion network supports high electronic mobility (electron-crystal behavior), while the disordered cations exhibit liquid-like dynamics that strongly scatter phonons, leading to ultralow κ_l.[30,31] Building on the phonon glass–electron crystal perception, this behavior has been described as a phonon liquid–electron crystal feature in disordered superionic conductors.

Ag_8GeTe_6 fits the argyrodite family, with the common formula $A^{m+}{}_{(12-n)/m}B^{n+}X^{2-}{}_6$ (A = Li, Ag, Cu; B = Si, Ge, Sn, and X = S, Se, Te; where m and n are the valence states of A and B).[32] Argyrodites typically adopt orthorhombic, hexagonal, or cubic structures at room temperature, and change to a high-symmetry cubic superionic phase at elevated temperatures.[33] In this phase, A-site cations are mobile and only weakly bonded to the rigid B–X sublattice. Their disordered distribution generates soft phonon modes and intense phonon scattering, resulting in ultralow κ_l.[34] While several groups have studied Se-based

DOI: 10.36838/IJHSR810.77

argyrodites for TE applications, Te-based systems have been much less explored.[28,30,35,36]

Here, we report n-type Ag_8GeTe_6. This compound crystallizes in a cubic phase with the space group $F\bar{4}3m$ above 244 K, and retains the *Fm3m* space group below this temperature.[37] Earlier reports described n-type Ag_8GeTe_6 with high ρ and poor *ZT*, largely due to poor sample density.[38] Subsequent studies by Charoenphakdee *et al.* and Zhu *et al.* demonstrated improved TE properties in p-type Ag_8GeTe_6 at elevated temperatures.[39,40] In the present work, n-type Ag_8GeTe_6 shows improved *ZT* near room temperature because of its ultralow κ_l, reduced ρ, and very high carrier mobility, μ. These results suggest that Ag_8GeTe_6 is a promising argyrodite TE material at room temperature, supported by its characteristic PLEC behavior.

Methods

Polycrystalline Ag_8GeTe_6 was synthesized by the melting method followed by annealing. High-purity elements Ag (shots, 99.99%), Ge (shots, 99.99%), and Te (shots, 99.99%) were weighed according to stoichiometric ratios and sealed in a vacuum quartz tube (~10^{-5} mbar). The sealed ampoule was heated to 1323 K over 12 h, held for 24 h, and then cooled to 873 K, where it was annealed for 72 h. The annealing stage was essential to suppress the creation of binary secondary phases. The obtained ingot was cleaned with sandpaper, ground into powder with an agate mortar and pestle, and then loaded into 10 mm graphite dies for spark plasma sintering (SPS211-LX, Dr. Sinter Lab). Sintering was carried out under ~10^{-3} mbar vacuum at 693 K for 5 min under a pressure of 45 MPa, yielding dense cylindrical pellets. The theoretical density of Ag_8GeTe_6 (7.02 g·cm^{-3}) was calculated from the refined lattice parameter (a = 11.5604 Å) and the crystallographic formula units per unit cell. The measured density (6.70 g·cm^{-3}, Archimedes method) corresponds to ~95.4% of the theoretical density. The density (*d*) of the sintered samples was determined using Archimedes' method. Polished specimens were cut for electrical and thermal transport measurements.

Phase purity and crystal structure were studied by X-ray diffraction (XRD, Rigaku Smartlab) in Bragg–Brentano geometry with Cu Kα radiation (λ = 1.5406 Å). Microstructure and chemical composition were characterized by field emission scanning electron microscopy with energy-dispersive spectroscopy (FESEM, Nova Nano SEM-450, JFEI, USA). Optical diffuse reflectance spectra were collected using a Cary 5000 UV–Vis–NIR spectrophotometer in the range 600–2400 nm at a scan rate of 600 nm min^{-1} at room temperature. The optical band gap was estimated using the Kubelka–Munk function, $F(R) = \alpha = (1-R)2/2R$, where α and R are the extinction and reflectance coefficients, respectively. Seebeck coefficient (S) and thermal conductivity (κ) were measured simultaneously from 2 to 380 K using the Quantum Design Physical Property Measurement System (PPMS) under helium atmosphere at ~10^{-5} Torr. Measurements were performed in continuous slow-warming mode using the steady-state heat flow method. Electrical contacts were completed with gold-coated copper leads attached by silver epoxy to samples of typical dimensions ~10 × 2 × 2 mm^3. Electrical resistivity (ρ), Hall coefficient (R), and heat capacity were also measured in the PPMS. Heat capacity was determined by the relaxation method using the two-τ model. The Hall carrier concentration (n) and mobility (μ) were calculated from $n = 1/eR$ and $\mu = R/\rho$, where e is the elementary charge.

Results and Discussion

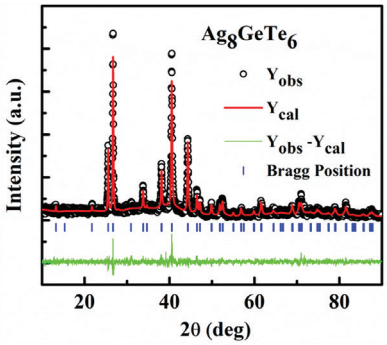

Figure 1: Room-temperature powder X-ray diffraction pattern of Ag_8GeTe_6 with Rietveld refinement. All reflections correspond to a cubic argyrodite structure (space group F$\bar{4}$3m) with no secondary phases detected, confirming high phase purity. The refined lattice parameter (a = 11.5604 Å) agrees with literature values, demonstrating successful synthesis of single-phase n-type Ag_8GeTe_6.

Figure 1 displays the XRD pattern of Ag_8GeTe_6 with a cubic structure (space group F$\bar{4}$3m). All reflections match ICDD card #04-006-4970. The nonappearance of minor peaks is confirmed by Rietveld refinement, and the refined lattice parameter a = 11.5604 Å agrees with previous reports, which indicates high sample purity.[37] The crystal structure of Ag_8GeTe_6 has been studied extensively. It undergoes a first-order, temperature-dependent phase transition near 244 K.[41] The room-temperature phase is cubic, similar to argyrodite compounds such as Cu_8GeSe_6 and Ag_8SiSe_6. The structure can be described as a Te^{2-} framework in which four tetrahedral $[GeTe_4]^{4-}$ units and four Te^{2-} ions fill tetrahedral voids, while Ag^+ cations partially occupy the remaining interstitial sites. Three crystallographically distinct Ag sites are present: 48*h* (0.422, 0.422, 0.223), 48*h* (0.473, 0.473, 0.218), and 96*i* (0.153, 0.445, 0.205), with occupancies of 1.00, 0.504, and 0.113, respectively. This disordered cation arrangement is typical of superionic semiconductors, where Ag ions can drift among partially occupied sites.

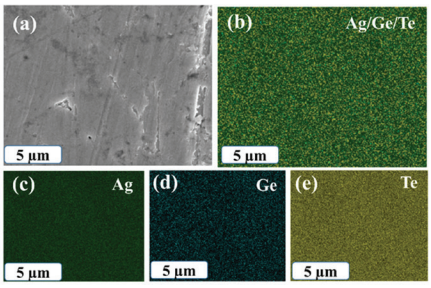

Figure 2: (a) SEM image of the prepared Ag_8GeTe_6 sample. EDS elemental mapping showing (b) combined distribution of all elements, and individual maps of (c) Ag, (d) Ge, and (e) Te. Uniform distribution of Ag, Ge, and Te is evident, and no impurity phases or agglomerations are observed. These results confirm compositional homogeneity and high-quality sample preparation essential for reliable transport measurements.

Figure 2 shows FESEM images and EDX elemental maps (Ag, Ge, Te) of Ag8GeTe6. The polished topmost surface of the bulk pellet appears clean, and the maps indicate uniform distributions of Ag, Ge, and Te with no visible secondary-phase agglomerates. EDX quantification yields an average composition of $Ag_{7.93}(\pm0.04)Ge_{1.00}(\pm0.02)Te_{6.05}(\pm0.06)$, indicating slight Ag deficiency and marginal Te enrichment within experimental uncertainty. This deviation from nominal stoichiometry is consistent with the observed n-type conduction, as Ag vacancies can contribute electron-donor–like behavior and modify carrier density in argyrodite chalcogenides.

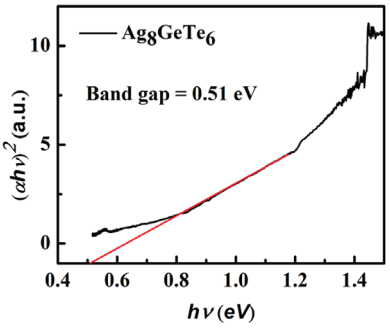

Figure 3: Tauc plot of $(\alpha h\nu)^2$ versus photon energy $h\nu$ for Ag_8GeTe_6 powder at room temperature. The optical band gap is obtained by linear extrapolation of the high-energy region (red line) using the Kubelka–Munk method. The extrapolated band gap of ~0.45 eV agrees with reported values, indicating semiconducting behavior with a narrow gap favorable for thermoelectric performance.

The optical band gap was estimated from the room-temperature diffuse reflectance spectrum (Figure 3). An analysis using $((\alpha h\nu)^2$ vs phonon energy $h\nu$ plot Eg ~0.45E_g eV, which is consistent with Bendorius *et al.*, who reported Eg ~0.43E_geV.[42]

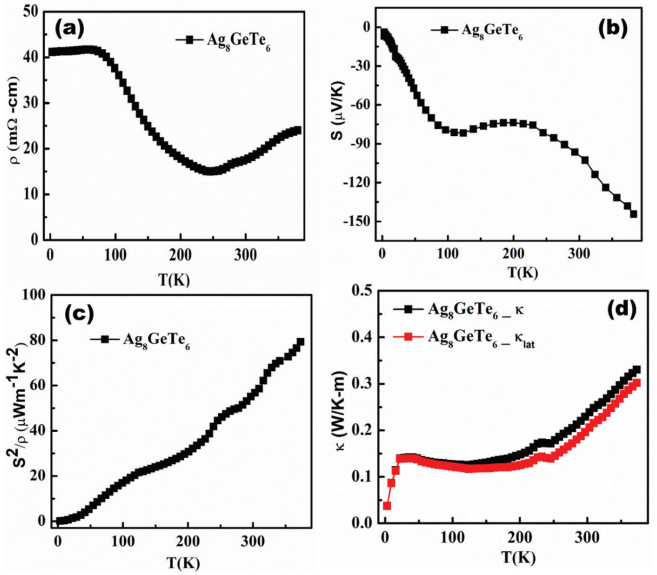

Figure 4: Temperature dependence of (a) electrical resistivity (ρ), (b) Seebeck coefficient (S), (c) power factor (S2/ρ), and (d) total thermal conductivity (κ, black symbols) and lattice contribution (κ_l, red symbols). Ag_8GeTe_6 exhibits a semiconducting-to-metallic transition near 244 K, n-type conduction throughout, and ultralow κ_l of 0.13–0.33 $W{\cdot}m^{-1}{\cdot}K^{-1}$. Together, these properties yield an enhanced power factor and confirm the phonon liquid–electron crystal behavior of the material.

To examine the transport behavior of Ag_8GeTe_6, the temperature dependences of ρ(T), S(T), and κ(T) are shown in Figure 4. The resistivity exhibits semiconducting behavior between 80 and 240 K, with ρ decreasing as T increases. In comparison, a metallic-like trend appears below 80 K. A first-order structural transition at ~240 K produces marked changes in all transport coefficients. As seen in Figure 4(a), ρ(T) shows a metallic-like temperature dependence above 240 K, which we attribute to a reduction in mobility (discussed below). The room-temperature resistivity, $\rho_{300}\sim10^{-2}$ Ω·cm, is higher than that of many state-of-the-art thermoelectrics. Yet, it is about two orders of magnitude less than earlier reports on p-type Ag_8GeTe_6, likely due to differences in stoichiometry and synthesis.

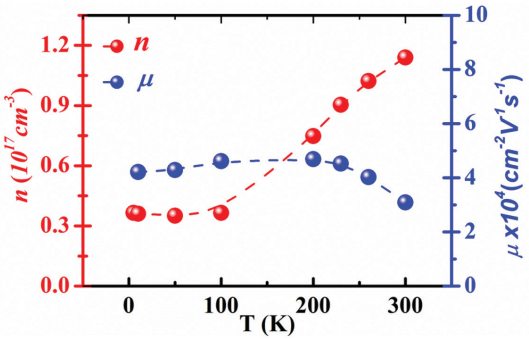

Figure 5: Temperature dependence of Hall mobility (μ) and carrier concentration (*n*) of Ag_8GeTe_6. Negative Hall coefficients confirm n-type conduction, while an exceptionally high room-temperature mobility (~3090 $cm^2{\cdot}V^{-1}{\cdot}s^{-1}$) and low carrier concentration (~10^{17} cm^{-3}) demonstrate decoupled charge and phonon transport. This combination explains the material's low resistivity and high thermoelectric potential.

An activation analysis using the Arrhenius relation between $ln\rho$ and 1/T below the transition (around 100 K) gives an intrinsic gap of approximately 0.023 eV. Hall measurements (Figure 5) show a negative Hall coefficient, indicating electrons as the majority carriers. The carrier concentration increases across the transition and reaches 1.14×10^{17} cm^{-3}, about one order of magnitude lower than previous reports.[40] In contrast, the Hall mobility is exceptionally high; the room-temperature value is μ ~3090 cm^2 V^{-1} s^{-1}, which is among the highest for known thermoelectric materials. This behavior is consistent with an "electron-crystal" response and aligns with room-temperature superionic chalcogenides such as Ag_8SiSe_6 and Ag_9GaSe_6. In the superionic state, the decrease of μ(T) points to enhanced carrier scattering from cation disorder.

The negative Seebeck coefficient S(T) over the whole temperature range designates that electrons are the main carriers, consistent with the Hall data. The n-type behavior of Ag_8GeTe_6 likely arises from a slight Ag deficiency, as suggested by the EDX results. As shown in Figure 4 (b), S(T) increases nearly linearly with temperature up to 120 K and reaches −82 μV/K, which is consistent with extrinsic transport inferred from ρ(T) at low temperature. In the semiconducting regime, S(T) becomes less negative and approaches ~−74 μV/K, which we attribute to a bipolar contribution associated with the small band gap. The onset of this effect is supported by the rise in carrier concentration to $n \sim 0.75\times10^{17}$ cm^{-3} at

DOI: 10.36838/IJHSR810.77

200 K (Figure 5). Above the superionic transition, the magnitude of S(T) increases and reaches −140 μV/K at 380 K. The inset of Figure 4 (c) shows the power factor S^2/ρ, which grows with temperature due to the increasing |S|. At 380 K, the power factor is 74 $\mu Wm^{-1}K^{-2}$, advanced than previous reports at a similar temperature.[39,40]

The total thermal conductivity κ(T) of Ag_8GeTe_6 lies between 0.13 and 0.33 $Wm^{-1}K^{-1}$ over 100 –380 K (Figure 4 (d)). The room-temperature value, κ_{300} = 0.24 $Wm^{-1}K^{-1}$, is markedly lower than that of many state-of-the-art thermoelectrics and most superionic TE chalcogenides. The lattice contribution, κ_l, was obtained by subtracting the electronic term, κ_e, from the total κ using the Wiedemann–Franz relation $\kappa_e = LT/\rho$, where the Lorenz number L was evaluated from the measured Seebeck coefficient using a standard SPB-based expression,[43]

$$L = 1.5 + \exp\left[-\frac{|S|}{116}\right] \quad \text{(Eq. 1)}.$$

At room temperature, κ_l ~0.20 $Wm^{-1}K^{-1}$ after the phase transition, which is lower than values reported for comparable superionic thermoelectrics.[23,44,45] With increasing temperature, κ_l (T) shows a slight rise across the transition and then remains nearly temperature independent up to 380 K. This contrasts with the conventional 1/T trend observed in crystalline solids at high temperature owing to Umklapp phonon scattering. The weak temperature dependence here is consistent with strong cation disorder and liquid-like motion of Ag^+ within a rigid anion framework, a hallmark of superionic systems.[28,30]

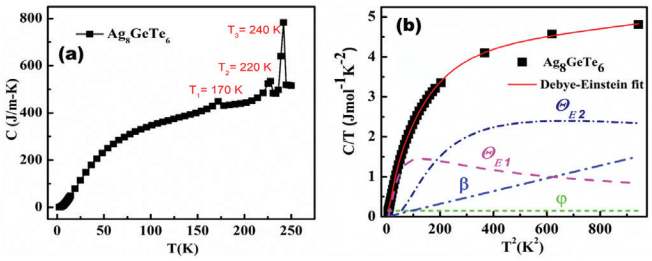

Figure 6: (a) Temperature dependence of heat capacity C(T)) for Ag_8GeTe_6. (b) Plot of C/T versus T^2 in the range 2–30 K. The red solid line shows the Debye–Einstein fit. Separate contributions from the electronic term (ϕ), the Debye term (β), and two Einstein modes (Θ_{E1}, Θ_{E2}) are also shown. The fit reveals two low-energy Einstein modes corresponding to localized Ag vibrations, consistent with a "phonon glass" state. These modes explain the suppressed lattice thermal conductivity and confirm the liquid-like dynamics of Ag^+ cations.

To investigate the source of the glass-like thermal conductivity at low temperature, we measured the heat capacity C(T) from 2 to 250 K (Figure 6 (a)). The C–T curve shows anomalies near ~170, ~220, and ~244 K. The higher-temperature features (~220 and ~244 K) are associated with symmetry changes reported for Ag_8GeTe_6. The weaker anomaly near ~170 K is discussed here as a likely precursor event involving partial ordering or local rearrangement of Ag^+ ions among partially occupied sites, indicating that cation dynamics evolve progressively with temperature. While this lowtemperature feature may subtly influence transport at cryogenic temperatures, the dominant thermoelectric behavior near room temperature is governed by the superionic disorder above the main transition.[41] The transitions ~220–240 K are associated with changes in crystal symmetry. We first fitted the low-temperature data using $C/T = \gamma + \beta T^2$, where γ is the electronic (Sommerfeld) coefficient, and β is the lattice term. The fit yielded a negative γ, which is unphysical. Given the presence of two sublattices, a rigid Ge–Te framework and liquid-like Ag cations, the data are better described by a combined Debye–Einstein model (Figure 6(b)).[46]

$$\frac{C}{T(x)} = \phi + \beta x + A\Theta_{E1}^2 x^{-\left(\frac{3}{2}\right)} \frac{e^{\frac{\Theta_{E1}}{\sqrt{x}}}}{\left(e^{\frac{\Theta_{E1}}{\sqrt{x}}} - 1\right)^2} + B\Theta_{E2}^2 x^{-\left(\frac{3}{2}\right)} \frac{e^{\frac{\Theta_{E2}}{\sqrt{x}}}}{\left(e^{\frac{\Theta_{E2}}{\sqrt{x}}} - 1\right)^2} \quad \text{(Eq. 2)}$$

Here x denotes T^2. The parameter ϕ represents the electronic contribution to the heat capacity, and β is the Debye term arising from acoustic phonons. Θ_{E1} and Θ_{E2} are Einstein temperatures that describe two local vibrational modes, and A and B are their weighting factors. Skutterudite thermoelectrics provide a well-known example of Debye–Einstein specific heat, where filler "rattler" atoms act as Einstein oscillators.[47] Using one Debye and two Einstein terms, the fitted temperature-dependent heatcapacity parameters are summarized in Table S3. The Debye temperature of Ag_8GeTe_6 is estimated as $\theta_D = \left(\frac{12\pi^4 NR}{5\beta}\right)^{1/3}$, where N=15 is the number of atoms per formula unit, and R=8.314 J $mol^{-1}K^{-1}$ is the gas constant. For Ag_8GeTe_6, we obtain θ_D=236 K. The Einstein temperatures are Θ_{E1}=29.24 K (≈2.52 meV) and Θ_{E2}=66.62 K (≈5.74 meV). Similar low-energy modes, often associated with weak chemical bonds, have been reported in skutterudites and other materials with liquid-like cation dynamics.[44] These modes enhance phonon scattering of the acoustic heat carriers and thereby suppress lattice thermal conductivity.

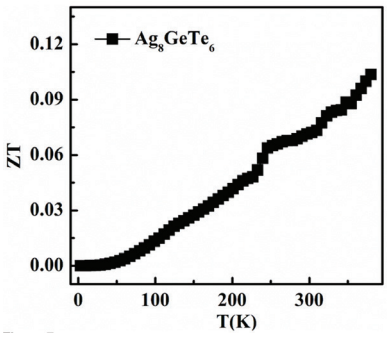

Figure 7: Temperature dependence of thermoelectric figure of merit (ZT) for Ag_8GeTe_6. A maximum ZT value of 0.10 is achieved at 380 K, nearly double previous reports for undoped Ag_8GeTe_6. This improvement arises from the synergy of high carrier mobility and ultralow lattice thermal conductivity, validating the design strategy for enhanced thermoelectric efficiency.

Using the measured ρ(T), S(T), and κ(T), we calculated the thermoelectric figure of merit ZT for Ag_8GeTe_6 (Figure 7). The maximum value is ZT_{max} =0.10 at 380 K, which is about twice the previously reported value for undoped Ag_8GeTe_6. The enhanced room-temperature ZT arises from the higher power factor S^2/ρ together with the very low thermal conductivity.

At room temperature, n-type Ag_8GeTe_6 from this work exhibits S = −101 μV/K, ρ = 0.018 Ω·cm, a power factor S^2/ρ = 56.84 $\mu Wm^{-1}K^{-2}$, κ = 0.24 $Wm^{-1}K^{-1}$, and a Hall mobility μ = 3090 $cm^2\ V^{-1}\ s^{-1}$, yielding ZT=0.074. Prior n-type Ag_8GeTe_6 reported by Fujikane *et al.* shows S = −123 μV/K and ρ = 0.19 Ω·cm, corresponding to a lower power factor of 7.96 $\mu Wm^{-1}K^{-2}$; at 770 K, that study lists κ=0.30 $Wm^{-1}K^{-1}$ and ZT=0.0014.[38] For p-type compositions, Charoenphakdee *et al.* reports S = 519 μV/K, ρ = 1.0 Ω·cm, S^2/ρ = 26.93 $\mu Wm^{-1}K^{-2}$, κ = 0.25 $Wm^{-1}K^{-1}$, and ZT = 0.035[39] while Zhu *et al.* demonstrates S = 580 μV/K, ρ = 1.0 Ω·cm, S^2/ρ = 33.64 $\mu Wm^{-1}K^{-2}$, κ = 0.27 $Wm^{-1}K^{-1}$, μ = 0.028 $cm^2\ V^{-1}\ s^{-1}$, and ZT = 0.037.[40] Compared with these literature values, the present n-type sample combines a much lower resistivity with an ultralow thermal conductivity and very high mobility, which results in the highest room-temperature power factor among the entries and a correspondingly improved ZT.

Conclusion

The structural, optical, and transport studies of Ag_8GeTe_6 demonstrate that this argyrodite compound combines ultralow lattice thermal conductivity with high carrier mobility. The observed phonon liquid–electron crystal characteristics arise from a rigid anion framework and disordered Ag cations, which generate strong phonon scattering and liquid-like dynamics. Compared with earlier reports, the present n-type samples show significantly reduced resistivity, higher power factor, and improved *ZT*, reaching 0.10 at 380 K. Although this *ZT* remains modest compared with state-of-the-art thermoelectrics, the results confirm the potential of Ag_8GeTe_6 as a model system for exploiting cation disorder and low-energy vibrational modes in argyrodite-type thermoelectrics. Future studies should focus on precise control of carrier concentration, Ag-site disorder (cation sublattice tuning), and defect engineering to further enhance the power factor and maximize ZT in Ag_8GeTe_6-based thermoelectric devices operating near room temperature.

Acknowledgments

We want to thank Prof. Woo Rin Lee for supporting this project.

References

1. T. Tritt, *Advances in Thermoelectric Materials I*, Elsevier Science, **2000**.
2. D. M. Rowe, *CRC Handbook of Thermoelectrics*, CRC Press, **1995**.
3. G. J. Snyder and E. S. Toberer, *Nat Mater,* **2008**, *7*, 105-114.
4. A. J. Minnich, M. S. Dresselhaus, Z. F. Ren and G. Chen, *Energy & Environmental Science*, **2009**, *2*, 466-479.
5. X. Shi, J. Yang, J. R. Salvador, M. Chi, J. Y. Cho, H. Wang, S. Bai, J. Yang, W. Zhang and L. Chen, *Journal of the American Chemical Society*, **2011**, *133*, 7837-7846.
6. R. Carlini, A. U. Khan, R. Ricciardi, T. Mori and G. Zanicchi, *Journal of Alloys and Compounds*, **2016**, *655*, 321-326.
7. H. Zhu, R. He, J. Mao, Q. Zhu, C. Li, J. Sun, W. Ren, Y. Wang, Z. Liu, Z. Tang, A. Sotnikov, Z. Wang, D. Broido, D. J. Singh, G. Chen, K. Nielsch and Z. Ren, *Nature Communications*, **2018**, *9*, 2497.
8. H. Zhu, J. Mao, Z. Feng, J. Sun, Q. Zhu, Z. Liu, D. J. Singh, Y. Wang and Z. Ren, *Science Advances*, **2019**, *5*, eaav5813.
9. G. S. Nolas, J. L. Cohn, G. A. Slack and S. B. Schujman, *Applied Physics Letters*, **1998**, *73*, 178-180.
10. X. Shi, J. Yang, S. Bai, J. Yang, H. Wang, M. Chi, J. R. Salvador, W. Zhang, L. Chen and W. Wong-Ng, *Advanced Functional Materials*, **2010**, *20*, 755-763.
11. Y. Pei, X. Shi, A. LaLonde, H. Wang, L. Chen and G. J. Snyder, *Nature*, **2011**, *473*, 66-69.
12. R. Chen, Y. Wang, L. Jiang, R. Min, H. Kang, Z. Chen, E. Guo, X. Yang, X. Jiang and T. Wang, *Materials Today Physics*, **2023**, *30*, 100957.
13. Y. Pei, H. Wang and G. J. Snyder, *Advanced Materials*, **2012**, *24*, 6125-6135.
14. J. Xin, Y. Tang, Y. Liu, X. Zhao, H. Pan and T. Zhu, *npj Quantum Materials*, **2018**, *3*, 9.
15. J. P. Heremans, B. Wiendlocha and A. M. Chamoire, *Energy & Environmental Science*, **2012**, *5*, 5510-5530.
16. L. Wu, X. Li, S. Wang, T. Zhang, J. Yang, W. Zhang, L. Chen and J. Yang, *NPG Asia Mater*, **2017**, *9*, e343.
17. Z. Du, J. He, X. Chen, M. Yan, J. Zhu and Y. Liu, *Intermetallics*, **2019**, *112*, 106528.
18. J. Hwang, J. H. Yun, K. Y. Lee, J.-S. Rhyee, J. Kim, S. Acharya, J. Kim, W. Kim, S. Kim and S.-J. Kim, *Materials Today Physics*, **2023**, *33*, 101053.
19. M. K. Jana, K. Pal, A. Warankar, P. Mandal, U. V. Waghmare and K. Biswas, *Journal of the American Chemical Society*, **2017**, *139*, 4350-4353.
20. A. F. May, E. S. Toberer, A. Saramat and G. J. Snyder, *Physical Review B*, **2009**, *80*, 125205-125201 - 125205-125212
21. S. Acharya, J. Pandey and A. Soni, *Applied Physics Letters*, **2016**, *109*, 133904.
22. S. Acharya, J. Pandey and A. Soni, *ACS Applied Energy Materials*, **2019**, *2*, 654-660.
23. H. Liu, X. Shi, F. Xu, L. Zhang, W. Zhang, L. Chen, Q. Li, C. Uher, T. Day and G. J. Snyder, *Nat Mater*, **2012**, *11*, 422-425.
24. M.-J. Guan, P.-F. Qiu, Q.-F. Song, J. Yang, D.-D. Ren, X. Shi and L.-D. Chen, *Rare Metals*, **2018**, DOI: 10.1007/s12598-018-1007-0.
25. T. Day, F. Drymiotis, T. Zhang, D. Rhodes, X. Shi, L. Chen and G. J. Snyder, *Journal of Materials Chemistry C*, **2013**, *1*, 7568-7573.
26. W. Mi, P. Qiu, T. Zhang, Y. Lv, X. Shi and L. Chen, *Applied Physics Letters*, **2014**, *104*, 133903.
27. X. Wang, P. Qiu, T. Zhang, D. Ren, L. Wu, X. Shi, J. Yang and L. Chen, *Journal of Materials Chemistry A*, **2015**, *3*, 13662-13670.
28. K. S. Weldert, W. G. Zeier, T. W. Day, M. Panthöfer, G. J. Snyder and W. Tremel, *Journal of the American Chemical Society*, **2014**, *136*, 12035-12040.
29. S. Bhattacharya, R. Basu, R. Bhatt, S. Pitale, A. Singh, D. K. Aswal, S. K. Gupta, M. Navaneethan and Y. Hayakawa, *Journal of Materials Chemistry A*, **2013**, *1*, 11289-11294.
30. B. K. Heep, K. S. Weldert, Y. Krysiak, T. W. Day, W. G. Zeier, U. Kolb, G. J. Snyder and W. Tremel, *Chemistry of Materials*, **2017**, *29*, 4833-4839.
31. B. Jiang, P. Qiu, H. Chen, Q. Zhang, K. Zhao, D. Ren, X. Shi and L. Chen, *Chemical Communications*, **2017**, *53*, 11658-11661.
32. W. F. Kuhs, R. Nitsche and K. Scheunemann, *Materials Research Bulletin*, **1979**, *14*, 241-248.
33. B. Jiang, P. Qiu, E. Eikeland, H. Chen, Q. Song, D. Ren, T. Zhang, J. Yang, B. B. Iversen, X. Shi and L. Chen, *Journal of Materials Chemistry C*, **2017**, *5*, 943-952.
34. S. Lin, W. Li, S. Li, X. Zhang, Z. Chen, Y. Xu, Y. Chen and Y. Pei, *Joule*, **2017**, *1*, 816-830.

DOI: 10.36838/IJHSR810.77

35. L. Wen, L. Siqi, G. Binghui, Y. Jiong, Z. Wenqing and P. Yanzhong, *Advanced Science*, **2016**, *3*, 1600196.
36. B. Jiang, P. Qiu, H. Chen, J. Huang, T. Mao, Y. Wang, Q. Song, D. Ren, X. Shi and L. Chen, *Materials Today Physics*, **2018**, *5*, 20-28.
37. F. Boucher, M. Evain and R. Brec, *Journal of Solid State Chemistry*, **1993**, *107*, 332-346.
38. M. Fujikane, K. Kurosaki, H. Muta and S. Yamanaka, *Journal of Alloys and Compounds*, **2005**, *396*, 280-282.
39. A. Charoenphakdee, K. Kurosaki, H. Muta, M. Uno and S. Yamanaka, *physica status solidi (RRL) – Rapid Research Letters*, **2008**, *2*, 65-67.
40. T. J. Zhu, S. N. Zhang, S. H. Yang and X. B. Zhao, *physica status solidi (RRL) – Rapid Research Letters*, **2010**, *4*, 317-319.
41. H. Kawaji and T. Atake, *Solid State Ionics*, **1994**, *70-71*, 518-521.
42. R. Bendorius, A. Iržikevičius, A. Kindurys and E. V. Tsvetkova, *Physica Status Solidi (a)*, **1975**, *28*, K125-K127.
43. H.-S. Kim, Z. M. Gibbs, Y. Tang, H. Wang and G. J. Snyder, *APL Materials*, **2015**, *3*, 041506-041501 - 041506-041505.
44. H. Liu, J. Yang, X. Shi, S. A. Danilkin, D. Yu, C. Wang, W. Zhang and L. Chen, *Journal of Materiomics*, **2016**, *2*, 187-195.
45. L. Li, Y. Liu, J. Dai, A. Hong, M. Zeng, Z. Yan, J. Xu, D. Zhang, D. Shan, S. Liu, Z. Ren and J.-M. Liu, *Journal of Materials Chemistry C*, **2016**, *4*, 5806-5813.
46. I. K. Dimitrov, M. E. Manley, S. M. Shapiro, J. Yang, W. Zhang, L. D. Chen, Q. Jie, G. Ehlers, A. Podlesnyak, J. Camacho and Q. Li, *Physical Review B*, **2010**, *82*, 174301-174301 - 174301-174308.
47. R. P. Hermann, R. Jin, W. Schweika, F. Grandjean, D. Mandrus, B. C. Sales and G. J. Long, *Physical Review Letters*, **2003**, *90*, 135505.

Authors

Juyoung Chang is a student at Seoul Foreign School. His research focuses on materials chemistry and solid-state physics, with a particular interest in the design and synthesis of high-performance thermoelectric compounds for sustainable energy applications.

Runyu Che is a high school researcher from Gyeonggi Suwon International School. He contributed to the structural and optical characterization of argyrodite compounds, with research interests in crystallography and renewable energy materials.

Beomjun Kim studies at Seoul International School. His research focuses on electronic transport and semiconductor materials, with a particular emphasis on mobility optimization in thermoelectric systems.

Chaemin Lee is a student at Phillips Exeter Academy. He participated in the analysis of temperature-dependent transport phenomena and is interested in applying physics and materials science to energy-efficient technologies.